

Molecular Beam Epitaxial Growth of Bi_2Te_3 and Sb_2Te_3 Topological Insulators on GaAs (111) Substrates: A Potential Route to Fabricate Topological Insulator p-n Junction

Zhaoquan Zeng^{1,7}, Timothy A. Morgan¹, Dongsheng Fan^{1,2}, Chen Li¹, Yusuke Hirono¹, Xian Hu¹, Joon Sue Lee³, Zhiming M. Wang^{1,4,5,8*}, Jian Wang^{3,6,8*}, Shuiqing Yu^{1,2}, Michael E. Hawkrige¹, Mourad Benamara¹, and Gregory J. Salamo¹

¹Arkansas Institute for Nanoscale Material Sciences and Engineering, University of Arkansas, Fayetteville, AR 72701, USA

²Department of Electrical Engineering, University of Arkansas, Fayetteville, AR 72701, USA

³The Center for Nanoscale Science and Department of Physics, The Pennsylvania State University, University Park, PA 16802, USA

⁴State Key Laboratory of Electronic Thin Films and Integrated Devices, University of Electronic Science and Technology of China, Chengdu 610054, China

⁵Engineering Research Center for Semiconductor Integrated Technology, Institute of Semiconductors, Chinese Academy of Science Beijing 100083, China

⁶International Center for Quantum Materials and State Key Laboratory for Mesoscopic Physics, School of Physics, Peking University, Beijing, 100871, China

E-mail: zhmwang@semi.ac.cn and jianwangphysics@pku.edu.cn

Abstract

High quality Bi_2Te_3 and Sb_2Te_3 topological insulators films were epitaxially grown on GaAs (111) substrate using solid source molecular beam epitaxy. Their growth and behavior on both vicinal and non-vicinal GaAs (111) substrates were investigated by reflection high-energy electron diffraction, atomic force microscopy, x-ray diffraction, and high resolution transmission electron microscopy. It is found that non-vicinal GaAs (111) substrate is better than a vicinal substrate to provide high quality Bi_2Te_3 and Sb_2Te_3 films. Hall and magnetoresistance measurements indicate that p type Sb_2Te_3 and n type Bi_2Te_3 topological insulator films can be directly grown on a GaAs (111) substrate, which may pave a way to fabricate topological insulator p-n junction on the same substrate, compatible with the fabrication process of present semiconductor optoelectronic devices.

Keywords: Topological Insulator, Atomic Force Microscopy, X-ray Diffraction, Transmission Electron Microscopy, Magnetoresistance

PACS: 68.35.Ct, 81.15.Hi, 68.55.aj, 72.20.My, 68.37.Lp

⁷ Present address: Electrical and Computer Engineering Department, The Ohio State University, Columbus, Ohio 43210, USA

⁸ Author to whom any correspondence should be addressed.

1. Introduction

Q_2Te_3 ($\text{Q} = \text{Bi}, \text{Sb}$) is a typical V-VI narrow gap semiconductor, having a rhombohedral unit cell that can be considered as three sets of groupings of -Te-Q-Te-Q-Te- planes, referred to as quintuple layers (QLs). Within the QL unit, the chemical bond provides the binding force, while the weak van der Waals (vdW) force acts between adjacent QLs. Q_2Te_3 is a traditional thermoelectric (TE) material (e.g. $ZT \approx 1$ for Bi_2Te_3 at 300 K), [1] that has caused attention in the past decade due to its superior TE performance. Recently, Q_2Te_3 -based research has increased because of the discovery of a new state of matter known as a three-dimensional (3D) “topological insulator” (TI). This material is insulating in bulk with a finite band gap but possesses a gapless surface state protected by time reversal symmetry (TRS), [2] which has been confirmed by angle-resolved photoemission spectroscopy (ARPES) [3-5] and transport measurements. [6-10] The emergence of TIs has brought an increase in the study of exotic quantum physics, such as Majorana fermions and magnetic monopoles, [11-13] which may pave the way for quantum computation applications. These investigations are also accelerating the development of spintronics due to the spin helical structure of the TI surface state. [14] Additionally, a very recent prediction shows that TI may be a promising candidate for use in high performance photodetectors in the terahertz (THz) to infrared (IR) frequency range because of high absorbance. [15]

With so many potential applications, it has become important to understand how to fabricate these materials. For example, molecular beam epitaxy (MBE) is one way to grow high quality TIs due to the advantages of ultra-high vacuum (UHV) background pressure and precise control of growth parameters. [5] In this communication, we have systematically investigated the fabrication of high-quality Q_2Te_3 films by MBE on GaAs substrates. Up to now, Si, SrTiO_3 , sapphire, and graphene have already been used as a substrate for the growth of Q_2Te_3 films by MBE. [3, 16, 17, 18] There have also been investigations on the MBE growth of Q_2Te_3 on a GaAs substrate. For example, Liu et al. demonstrated epitaxial growth of both Bi_2Te_3 and Bi_2Se_3 films on GaAs (100) directly by van der Waals epitaxy (vdWe). [19] They reported that rotation domains formed in the TIs films due to the lattice symmetry mismatch between the hexagonal lattices of Bi_2Te_3 and the cubic symmetry of the GaAs (001) surface. [19] The vdWe growth method has also been used for the growth of Bi_2Se_3 on a vicinal Si (111) surface. [20] However, an amorphous intermediate layer formed in this approach which of course is not good for the coupling of spins between the substrate and the TI film, and could hinder the integration of TIs on

present semiconductor optoelectronic devices. On the other hand, GaAs (111) should be a good substrate to realize coherent heteroepitaxy of Q_2Te_3 due to the lattice symmetry. For example, He et al. focused on the measurement of the magnetoresistance properties of Bi_2Te_3 thin films grown on semi-insulating GaAs (111) with ZnSe as a buffer layer [21] while Richardella et al. demonstrated coherent heteroepitaxy of Bi_2Se_3 on GaAs (111)B. [22]

In this paper, we have investigated the growth and behavior of Q_2Te_3 on both vicinal and non-vicinal GaAs (111) (V-GaAs (111) and Nv-GaAs(111)) substrates by reflection high-energy electron diffraction (RHEED), atomic force microscopy (AFM), x-ray diffraction (XRD) and high resolution transmission electron microscopy (HRTEM). Together with Hall and magnetoresistance (MR) measurements, results indicate that p type Sb_2Te_3 and n type Bi_2Te_3 topological insulator films can be directly grown on a GaAs (111) substrate, enhancing the opportunity to fabricate topological insulator p-n junctions. [23]

2. Experimental

A Riber 32P solid source MBE system was used to grow Q_2Te_3 films on epi-ready GaAs (111) substrates. The growth chamber is equipped with a RHEED (Staib) and a transmission optical system (kSA BandiT) monitoring the substrate band edge to give accurate growth temperature down to 150 °C. High purity 6N Bi, Sb and Te sources were evaporated to provide the beam fluxes for the film growth with a ratio of about 1 : 12. The morphology of as-grown films were quenched by turning off the manipulator heater right after the growth, and a Veeco ambient AFM was used to characterize the sample surface. High resolution XRD (HRXRD) was performed on a PANalytical X'Pert MRD system equipped with a parabolic mirror and PIXcelTM detector. The interface was characterized on FEI Titan 80-300 TEM. The Hall bar structure for transport measurement was fabricated using standard photo-lithography method (see Supporting Information for more details).

The Q_2Te_3 films were grown on GaAs (111)A or GaAs (111)B substrates. As a result, two kinds of different RHEED evolutions were observed during growth due to the difference between A and B planes of GaAs (111) (see Supporting Information for more details). As a comparison, both V-GaAs (111) and Nv-GaAs(111) substrates were used as substrates for growth of Q_2Te_3 films. This is motivated by the fact that a vicinal Si (111) substrate was observed to improve the quality of Bi_2Se_3 epitaxial films grown by vdWe. [20] After deoxidizing GaAs substrates at 610 °C, a two steps growth method, i.e. a high temperature GaAs buffer layer growth at 590 °C and a low temperature Q_2Te_3 film growth at 250 °C, was performed. More than ten kinds of different samples were investigated, and here we will show the data from the six kinds of samples as shown in table 1. Sample A (200 nm Bi_2Te_3 /V-GaAs (111)A-3°) and sample B (400 nm

Sb₂Te₃/V-GaAs (111)A-3°) was a 200 nm thick Bi₂Te₃ film and a 400 nm thick Sb₂Te₃ film, respectively, grown on V-GaAs (111)A substrate (3° miscut) with a 330 nm thick GaAs buffer layer. samples C and D were grown on the same moly block with the same thick GaAs buffer layer (3 nm) and Bi₂Te₃ film (30 nm) on V-GaAs (111)A and Nv-GaAs (111)A, respectively. Samples E (200 nm thick Bi₂Te₃) and F (400 nm thick Sb₂Te₃) were grown on V-GaAs (111)B substrate with a 330 nm thick GaAs buffer layer.

3. Results and Discussion

3.1 Surface morphology studies with atomic force microscopy

Figure 1 shows a set of AFM images, which reveal the different growth modes of Q₂Te₃ films observed on both V-GaAs (111) and Nv-GaAs(111) substrates. Figure 1a is the AFM image of sample A (200 nm Bi₂Te₃/V-GaAs (111)A-3°). The big terraces and steps run nearly parallel. In most areas, about 1 μm wide terraces and 35 nm high steps can be found. The root-mean-square (RMS) roughness is about 8 nm for 5×5 μm² area. Furthermore, small steps with height of about 1 nm were observed on the flat terrace as seen in figures 1(b-c) (500×500 nm²), consistent with a single QL thickness for each step. This surface morphology covers the entire sample surface based on more AFM measurements at the different positions on the surface of sample A. Sample B (400 nm Sb₂Te₃/V-GaAs (111)A-3°) shows the similar surface morphology as shown in figure 1d. Obviously, this is a typical step-bunched surface, [24] which forms with the big steps and terraces through a step-flow growth mode. Such surface morphology is very different compared to reported result of spiral growth. [20, 25] In order to avoid concerns over variation in the thickness of GaAs buffer layer or Q₂Te₃ film, both samples C (30 nm Bi₂Te₃/V-GaAs (111)A-3°) and D (30 nm Bi₂Te₃/Nv-GaAs (111)A) were grown on the same molybdenum block simultaneously using the same thick GaAs buffer layer (3 nm) and Q₂Te₃ (30 nm) films. As shown in figure 1e, sample C still shows an initial step-bunched surface. However, spiral growth was observed for sample D as shown in figures 1(f-h). For the as-grown Q₂Te₃ film, AFM investigations indicate that a V-GaAs (111) substrate is conducive to the formation of a step bunched surface through the tendentious step-flow growth induced by the high density of steps providing the high energy barrier to grow over the steps in its surface. [26] Nv-GaAs (111) substrates sustain a smooth surface during spiral growth or partial step-flow growth due to the lower step density associated with non-vicinal substrate surface (see more AFM investigation results in the Supporting Information).

3.2 Structural studies with x-ray diffraction and transmission electron microscopy

To determine the crystal quality and epitaxial orientation of as-grown Q₂Te₃ films, XRD was performed. Figures 2(a-b) are the 2θ-ω scans within 0-80° range for samples E (200 nm

Bi₂Te₃/V-GaAs (111)B-3°) and F (400 nm Sb₂Te₃/V-GaAs (111)B-3°). Only Q₂Te₃ (003) and GaAs (111) families of reflections were observed, indicating the high c-axis orientation of Q₂Te₃ films along GaAs [111] direction, i.e. Q₂Te₃ (001)//GaAs (111). Compared with the peak position of GaAs substrates, the QL thickness (equals to 1/3 of lattice constant c) was given by $d_{QL}=1.011$ nm for Bi₂Te₃ and $d_{QL}=1.007$ nm for Sb₂Te₃, respectively, consistent with the RHEED observation results that the Q₂Te₃ lattice is fully relaxed. The full-width-half-maximum (FWHM) is 0.09° and 0.014° for Bi₂Te₃ (006) and Sb₂Te₃ (00,15), respectively, as shown in figures 2(c-d), indicating high-quality growth. To distinguish the subtle difference of as-grown Q₂Te₃ films, reciprocal space mapping (RSM) was performed on samples F (400 nm Sb₂Te₃/V-GaAs (111)B-3°), C (30 nm Bi₂Te₃/V-GaAs (111)A-3°) and D (30 nm Bi₂Te₃/Nv-GaAs (111)A). The RSM results of symmetric planes in figures 2(e-g) distinctly demonstrated the tilted angle of 0.055°, 0.046° and 0.002° between Q₂Te₃ (00,18) and GaAs (222), for samples F, C and D, respectively, indicating higher c-axis epitaxial orientation than vdWe on a vicinal substrate. [21] For these three samples, Sample D grown on non-vicinal substrate has a better c-axis orientation than samples C and F. The RSM result of non-symmetric planes of GaAs (440) and Bi₂Te₃ ($\bar{2}27$) for sample D in figure 2h presents the in-plane lattice mismatch between Bi₂Te₃ film and GaAs (111) substrate is around 9.3%, which is consistent with the RHEED observation of small critical thickness. Besides, the peak of sample F grown on vicinal substrate with thick GaAs buffer layer is much broader than that of samples C and D, indicating worse crystalline quality. The substrate miscut dependence of the tilted orientation angles for these three samples proves that as-grown Q₂Te₃ films are sensitive to the surface lattice orientation of the substrates and V-GaAs (111) substrates can reduce their crystalline quality through the unfavorable step bunching process.

To further clarify the effect of V-GaAs (111) substrates on the crystal quality of as-grown Q₂Te₃ film, we investigated the interface between Q₂Te₃ films and GaAs buffer layer for these three samples by HRTEM. Figure 3(a) gives the HRTEM images of sample F. It is obvious that the interface is disordered and a lot of defects were formed in both the GaAs buffer layer and Sb₂Te₃ film. Furthermore, the fast Fourier transform (FFT) analysis near the interface confirmed the RSM result that there is a small tilted angle of about 0.055° between the Sb₂Te₃ film and GaAs (111) substrate. For sample C, a similar result is observed in figure 3(b), i.e. disordered interface and tilted orientation, except for that fewer defects were formed due to the thinner GaAs buffer layer. In contrast, both a sharp interface and nearly parallel orientation were found for sample D, as shown in figures 3(c-d). Based on these observations, we can conclude that an Nv-GaAs (111) substrate is better to use than a vicinal substrate in order to fabricate high quality Q₂Te₃ films on GaAs (111) substrate.

3.3 Transport measurements of Q_2Te_3 thin films

In order to demonstrate the topological insulator behavior of as-grown Q_2Te_3 films, transport measurements were also performed. As expected, all the Sb_2Te_3 films show p type conducting behavior, whereas, all the Bi_2Te_3 films show n type conducting behavior. Figure 4 shows the typical transport measurement results of Q_2Te_3 films on GaAs (111)B (see the transport data for Q_2Te_3 films on GaAs (111)A in Supporting Information). Nonlinear Hall behavior was observed over 20 kOe for both samples E (200 nm $\text{Bi}_2\text{Te}_3/\text{V-GaAs (111)B-3}^\circ$) and F (400 nm $\text{Sb}_2\text{Te}_3/\text{V-GaAs (111)B-3}^\circ$) at 1.8 K, as shown in figures 4(a-b), which is likely an indication of more than one transport channel (surface and bulk). Based on the linear behavior below 20 kOe, the carrier density and mobility can be estimated as $7.81 \times 10^{18} \text{ cm}^{-3}$ and $959 \text{ cm}^2/\text{Vs}$, $9.13 \times 10^{18} \text{ cm}^{-3}$ and $781 \text{ cm}^2/\text{Vs}$ for samples E and F, respectively, indicating good electrical properties. [3, 31] Magnetoresistance (MR) measurements were performed for three different directional fields up to 80 kOe. For the perpendicular field (H), the MR increases to 1.73 and 1.56 times for samples E and F at 1.8 K, respectively, over the range of 0 to 80 kOe; linear MR was observed above 20 kOe, which may be attributed to the quantum linear MR (QLMR) of the surface states, [27] as shown in figures 4(c-d). For the parallel field in figures 4(e-f), MR increases to 1.15~1.30 times, which is smaller than the MR in perpendicular field. In a close-up view as shown in figure 4g, a clear MR dip was observed for sample E in perpendicular field, between -2 and 2 kOe, which can be attributed to the weak anti-localization effect (WAL). [8, 21, 28, 29, 30, 31] Meanwhile, the temperature dependence of MR for sample F has an upturn below 4 K with fields 20 and 80 kOe, as shown in figure 4h, which is reminiscent of the electron-electron interaction in TI films. [8]

4. Conclusion

In summary, we have successfully demonstrated the MBE growth of Q_2Te_3 topological insulator films directly on GaAs (111) substrates. Similar to the results reported by Liu et al., [25] spiral growth mode was observed for Q_2Te_3 films on Nv-GaAs (111)A substrate. However, an step-bunched surface was observed for Q_2Te_3 films on V-GaAs (111)A substrates. Both XRD and HRTEM results indicate that the Nv-GaAs (111) substrate is better than a vicinal substrate to provide high quality Q_2Te_3 films. The tilted angle between Q_2Te_3 film and GaAs (111) substrate may be related to the misfit dislocation with a nonzero net out-of-plane Burgers vector component since Nagai's steps model is not applicable here due to the large lattice mismatch, [32, 33] and more interface investigations need to be done to establish the tilting mechanism in this kind of high-misfit heteroepitaxial systems. The observation of linear MR and WAL provides proofs for the TI behavior of as-grown Q_2Te_3 films. [10, 27] Hall effect measurements show that unintentional doping happens to as-grown Q_2Te_3 films: Sb_2Te_3 films always show p type

conducting behavior, whereas, Bi_2Te_3 films always show n type conducting behavior, creating the potential to fabricate topological p-n junction on the same GaAs (111) substrate. Further, it may pave a way to integrate TI-based devices with present semiconductor optoelectronic devices, generating brand-new multifunction device.

Acknowledgment

The authors gratefully acknowledge the NSF financial support through Grant No. DMR-0520550, the National Basic Research Program of China (Grant No. 2012CB921300), the National Natural Science Foundation of China (Grant No. 11174007), the Penn State MRSEC under NSF grant DMR-0820404. We are grateful to Moses H. W. Chan and Meenakshi Singh for the help in the transport measurement.

References

- [1] N. Peranio, O. Eibl, J. Nurnus 2006 *J. Appl. Phys.* 100 114306
- [2] H. J. Zhang, C. X. Liu, X. L. Qi, X. Dai, Z. Fang, S. C. Zhang 2009 *Nat. Phys.* 5 438
- [3] Y. Y. Li, G. A. Wang, X. G. Zhu, M. H. Liu, C. Ye, X. Chen, Y. Y. Wang, K. He, L. L. Wang, X. C. Ma, H. J. Zhang, X. Dai, Z. Fang, X. C. Xie, Y. Liu, X. L. Qi, J. F. Jia, S. C. Zhang, Q. K. Xue 2010 *Adv. Mater.* 22 4002
- [4] Y. L. Chen, J. G. Analytis, J. H. Chu, Z. K. Liu, S. K. Mo, X. L. Qi, H. J. Zhang, D. H. Lu, X. Dai, Z. Fang, S. C. Zhang, I. R. Fisher, Z. Hussain, Z. X. Shen 2009 *Science* 325 178
- [5] X. Chen, X. C. Ma, K. He, J. F. Jia, Q. K. Xue, 2011 *Adv. Mater.* 23 1162
- [6] D. S. Kong, W. H. Dang, J. J. Cha, H. Li, S. Meister, H. L. Peng, Z. F. Liu, Y. Cui 2010 *Nano. Lett.* 10 2245
- [7] D. X. Qu, Y. S. Hor, J. Xiong, R. J. Cava, N. P. Ong 2010 *Science* 329 821
- [8] J. Wang, A. M. DaSilva, C. Z. Chang, K. He, J. K. Jain, N. Samarth, X. C. Ma, Q. K. Xue, M. H. W. Chan 2011 *Phys. Rev. B* 83 245438
- [9] H. Steinberg, J. B. Laloe, V. Fatemi, J. S. Moodera, P. Jarillo-Herrero 2011 *Phys. Rev. B* 84 233101
- [10] J. Chen, H. J. Qin, F. Yang, J. Liu, T. Guan, F. M. Qu, G. H. Zhang, J. R. Shi, X. C. Xie, C. L. Yang, K. H. Wu, Y. Q. Li, L. Lu 2010 *Phys. Rev. Lett.* 105 176602
- [11] X. L. Qi, S. C. Zhang 2010 *Phys. Today* 63 33
- [12] M. Z. Hasan, J. E. Moore 2011 *Ann. Rev. Cond. Mat. Phys.* 2 55
- [13] M. Z. Hasan, C. L. Kane 2010 *Rev. Mod. Phys.* 82 3045

- [14] D. Hsieh, Y. Xia, D. Qian, L. Wray, J. H. Dil, F. Meier, J. Osterwalder, L. Patthey, J. G. Checkelsky, N. P. Ong, A. V. Fedorov, H. Lin, A. Bansil, D. Grauer, Y. S. Hor, R. J. Cava, M. Z. Hasan 2009 *Nature* 460 1101
- [15] X. A. Zhang, J. Wang, S. C. Zhang 2010 *Phys. Rev. B* 82 245107
- [16] G. H. Zhang, H. J. Qin, J. Teng, J. D. Guo, Q. L. Guo, X. Dai, Z. Fang, K. H. Wu 2009 *Appl. Phys. Lett.* 95 053114
- [17] J. S. Zhang, C. Z. Chang, Z. C. Zhang, J. Wen, X. Feng, K. Li, M. H. Liu, K. He, L. L. Wang, X. Chen, Q. K. Xue, X. C. Ma, Y. Y. Wang 2011 *Nat. Commun.* 2 574
- [18] C. L. Song, Y. L. Wang, Y. P. Jiang, Y. Zhang, C. Z. Chang, L. L. Wang, K. He, X. Chen, J. F. Jia, Y. Y. Wang, Z. Fang, X. Dai, X. C. Xie, X. L. Qi, S. C. Zhang, Q. K. Xue, X. C. Ma 2010 *Appl. Phys. Lett.* 97 143118
- [19] X. Liu, D. J. Smith, J. Fan, Y. H. Zhang, H. Cao, Y. P. Chen, J. Leiner, B. J. Kirby, M. Dobrowolska, J. K. Furdyna 2011 *Appl. Phys. Lett.* 99 171903
- [20] H. D. Li, Z. Y. Wang, X. Kan, X. Guo, H. T. He, Z. Wang, J. N. Wang, T. L. Wong, N. Wang, M. H. Xie 2010 *New. J. Phys.* 12 103038
- [21] H. T. He, G. Wang, T. Zhang, I. K. Sou, G. K. L. Wong, J. N. Wang, H. Z. Lu, S. Q. Shen, F. C. Zhang 2011 *Phys. Rev. Lett.* 106 166805
- [22] A. Richardella, D. M. Zhang, J. S. Lee, A. Koser, D. W. Rench, A. L. Yeats, B. B. Buckley, D. D. Awschalom, N. Samarth 2010 *Appl. Phys. Lett.* 97 262104
- [23] J. Wang, X. Chen, B. F. Zhu, S. C. Zhang 2012 *Phys. Rev. B* 85 235131
- [24] M. Shinohara, N. Inoue 1995 *Appl. Phys. Lett.* 66 1936
- [25] Y. Liu, M. Weinert, L. Li 2012 *Phys. Rev. Lett.* 108 115501
- [26] Y. Takagaki, B. Jenichen 2012 *Semicond. Sci. Tech.* 27 035015
- [27] H. Tang, D. Liang, R. L. J. Qiu, X. P. A. Gao 2011 *Acs Nano* 5 7510
- [28] H. Z. Lu, J. R. Shi, S. Q. Shen 2011 *Phys. Rev. Lett.* 107 076801
- [29] Y. S. Kim, M. Brahlek, N. Bansal, E. Edrey, G. A. Kapilevich, K. Iida, M. Tanimura, Y. Horibe, S. W. Cheong, S. Oh 2011 *Phys. Rev. B* 84 073109
- [30] J. Wang, C. Z. Chang, H. D. Li, K. He, D. M. Zhang, M. Singh, X. C. Ma, N. Samarth, M. H. Xie, Q. K. Xue, M. H. W. Chan 2012 *Phys. Rev. B* 85 045415
- [31] Y. Takagaki, A. Giussani, K. Perumal, R. Calarco, K.-J. Friedland 2012 *Phys. Rev. B* 86 125137
- [32] H. Nagai 1974 *J. Appl. Phys.* 45 3789
- [33] F. Riesz 1996 *J. Vac. Sci. Technol. A* 14 425

Table**Table 1.** Samples category of Q_2Te_3 on GaAs (111) substrate

| Sample. | Q_2Te_3 & Thickness | Buffer Layer & Thickness | Substrate[a] | Misalignment Angle | Conduction Type |
|----------|--|---------------------------------------|---|-----------------------------------|-----------------|
| A | Bi_2Te_3 & 200 nm | GaAs (111)A & 330 nm | N type V-GaAs (111)A \rightarrow ($\bar{2}11$) | 3° | n |
| B | Sb_2Te_3 & 400 nm | GaAs (111)A & 330 nm | N type V-GaAs (111)A \rightarrow ($\bar{2}11$) | 3° | p |
| C | Bi_2Te_3 & 30 nm | GaAs (111)A & 3 nm | N type V-GaAs (111)A \rightarrow ($\bar{2}11$) | 3° | / |
| D | Bi_2Te_3 & 30 nm | GaAs (111)A & 3 nm | Semi-insulating Nv-GaAs (111)A | $\pm 0.1^\circ$ | n |
| E | Bi_2Te_3 & 200 nm | GaAs (111)B & 330 nm | N type V-GaAs (111)B \rightarrow ($2\bar{1}\bar{1}$) | 3° | n |
| F | Sb_2Te_3 & 400 nm | GaAs (111)B & 330 nm | N type V-GaAs (111)B \rightarrow ($2\bar{1}\bar{1}$) | 3° | p |

[a]V-GaAs (111) substrate was made by AXT Inc., whereas, Nv-GaAs(111) was made by Wafer Technology Ltd.

Figure Captions:

Figure 1. AFM images of surface morphology for as-grown Q_2Te_3 films on GaAs (111)A. a) Sample A in $5 \times 5 \mu\text{m}^2$, b) Sample A in $500 \times 500 \text{ nm}^2$, c) the line profile corresponding to the line in b), d) Sample B in $5 \times 5 \mu\text{m}^2$, e) Sample C in $5 \times 5 \mu\text{m}^2$, f) Sample D in $5 \times 5 \mu\text{m}^2$, g) Sample D in $2 \times 2 \mu\text{m}^2$, h) the line profile corresponding to the line in g).

Figure 2. XRD patterns of as-grown Q_2Te_3 films. a) 2θ - ω scan of sample E, b) 2θ - ω scan of sample F, c) ω scan of sample E, d) ω scan of sample F, e) RSM mapping of sample F between GaAs [222] and Sb_2Te_3 [0,0,18], f) RSM mapping of sample C between GaAs [222] and Bi_2Te_3 [0,0,18], g) RSM mapping of sample D between GaAs [222] and Bi_2Te_3 [0,0,18], h) RSM mapping of sample D between GaAs [440] and Bi_2Te_3 [$\bar{2}$,2,27]. For RSM mapping, the Bartels monochromator was removed, hence $\text{Cu-K}_{\alpha 1}$ and $\text{K}_{\alpha 2}$ peaks are visible and a large $\Delta\lambda$ streak is present through the substrate reflection.

Figure 3. Cross-sectional HRTEM images of as-grown $\text{Q}_2\text{Te}_3/\text{GaAs}$ (111) heterostructures. a) Sample F with the zone axis of GaAs [$10\bar{1}$], b) Sample C with the zone axis of GaAs [$10\bar{1}$], c)

Sample D with the zone axis of GaAs $[10\bar{1}]$, d) Sample D with the zone axis of GaAs $[11\bar{2}]$. The white arrows indicate the interface, the red arrows point defects, and the right rows show the corresponding FFT images of samples F, C and D; For all the FFT images, we see two sets of diffraction patterns with different symmetry: one is from GaAs substrate, and the other is from Q_2Te_3 film.

Figure 4. Transport properties of as-grown Q_2Te_3 films. a,b) Hall resistance versus magnetic field (black solid line) at 1.8 K for samples E and F, respectively, and the red solid line is the linear fitting one, c,d) MR change in perpendicular magnetic field (black solid line) for samples E and F, respectively, and the red dashed line is the linear fitting one, e,f) MR change in both perpendicular and parallel magnetic fields configuration for samples E and F, g) Magnetoresistivity in perpendicular magnetic field between -2 and 2 kOe for sample E, h) MR change versus temperature in perpendicular magnetic field for sample F. We use three different magnetic field configurations, H_\perp denote magnetic field perpendicular to the surface of the thin film, while H_\parallel and H_\parallel' denote an in-plane magnetic field perpendicular to and parallel to the excitation current, respectively.

Figure 1

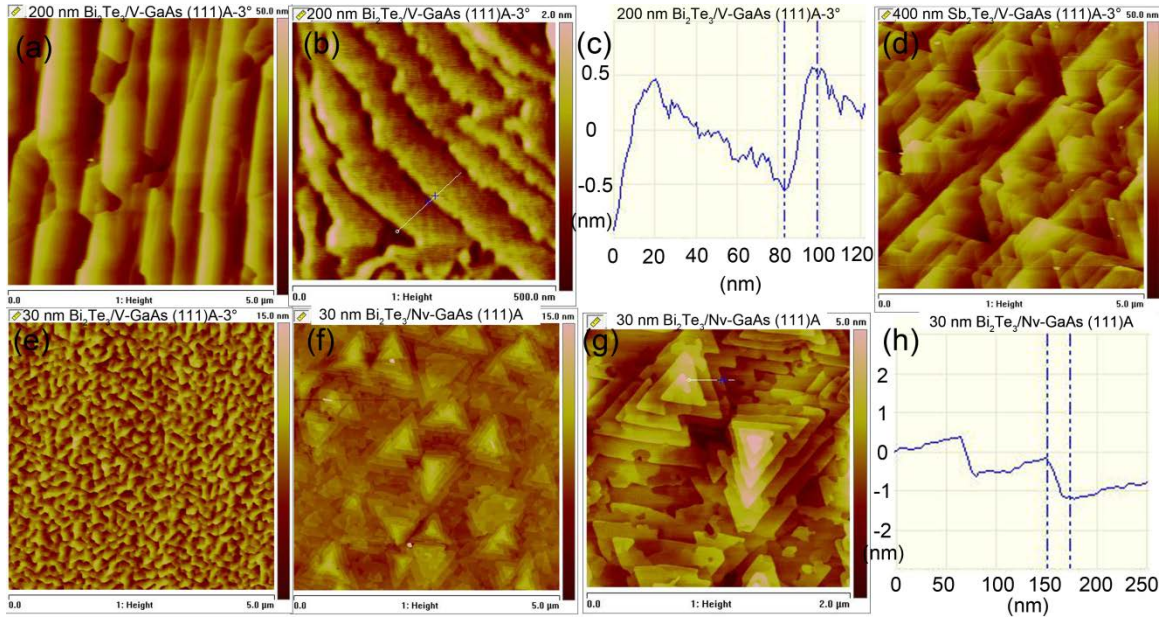


Figure 2

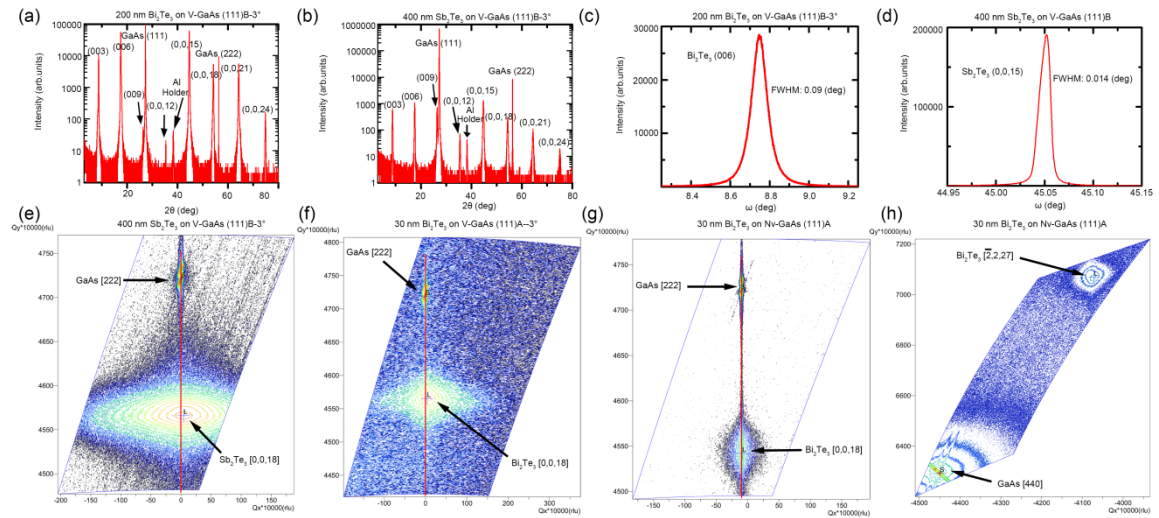


Figure 3

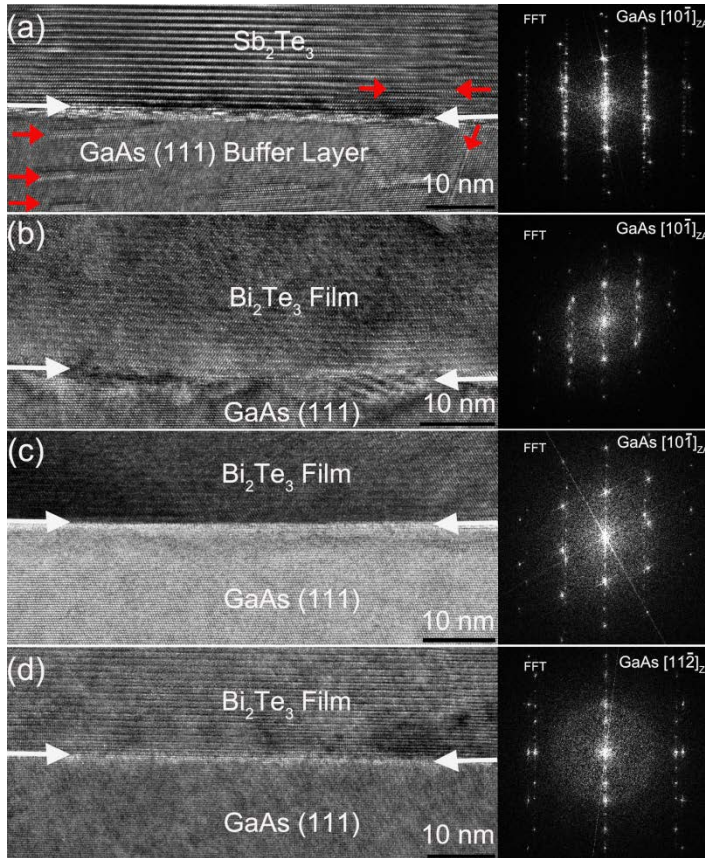
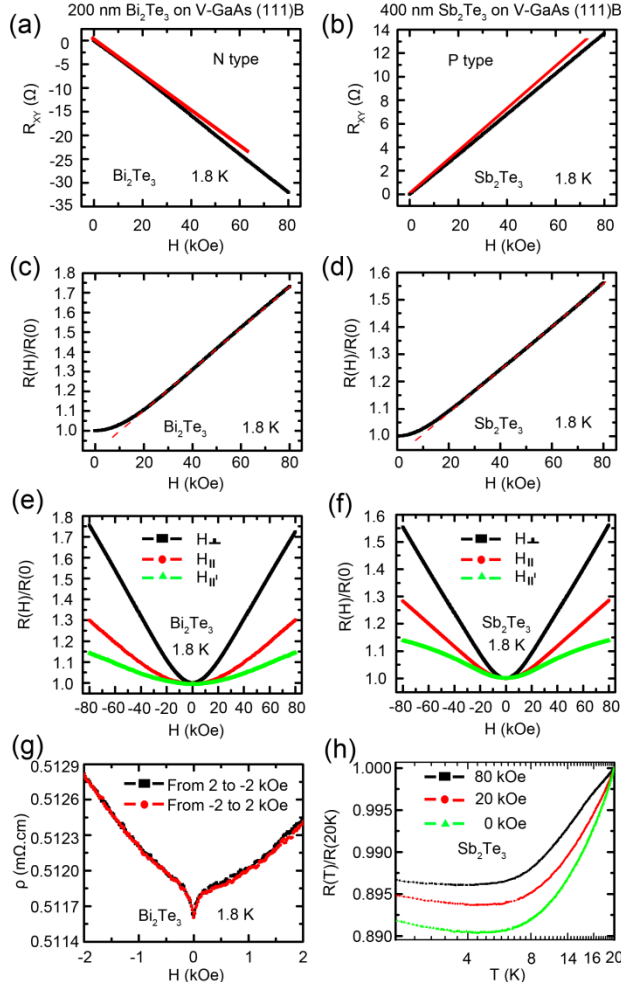


Figure 4



Support Information

1. RHEED Evolution:

Figure 1S shows the typical RHEED evolution for Bi_2Te_3 films grown on GaAs (111)A substrates. Figure 1S(a-b) show the RHEED patterns of GaAs (111)A surface after deoxidizing and growth of GaAs buffer layer. After several minutes at deoxidizing temperature of 590 °C, the 2×2 reconstruction gradually appears, and it exists during the whole GaAs buffer layer growth. The clear 2×2 reconstruction and sharp streak indicate that a typical GaAs (111)A clean surface is formed^[1]. While the substrate was cooled down to 250 °C, the 2×2 RHEED pattern disappeared, and 1×1 pattern appeared (figure 1S(c-d)). It can be attributed to the predeposition

of Te, providing a Te rich growth condition for Bi_2Te_3 . When the Bi shutter was open, the sharp streak became dim and shrank inside slowly (not shown here), which indicated the epitaxial growth of c-axis oriented Bi_2Te_3 film. As Bi_2Te_3 grew, the streaky RHEED patterns became sharp, indicating a flat surface. After epilayer growth for scores of nms, a set of sharp streaky pattern with clear Kikuchi lines was observed (figure 1S(e-f)), suggesting good crystallinity. It should be mentioned that the 1×1 surface persisted during the whole epilayer growth. Comparing the RHEED patterns of GaAs (111)A and Bi_2Te_3 epitaxy film, it can be concluded that relaxed Bi_2Te_3 (001) film has been grown on GaAs (111)A surface with an overlapped in-plane epitaxial relationship of Bi_2Te_3 $[10\bar{1}0]//\text{GaAs}$ $[1\bar{1}2]$ and Bi_2Te_3 $[1\bar{1}20]//\text{GaAs}$ $[10\bar{1}]$.

Figure 2S shows the typical RHEED evolution for Bi_2Te_3 grown on GaAs (111)B substrates. Figure 2Sa shows the RHEED patterns of GaAs (111)B surface right after deoxidization at 590 °C, a typical $\sqrt{19} \times \sqrt{19}$ reconstructed surface of GaAs (111)B at high temperature^[1] (the other direction is not shown here). During cooling down to 250 °C, a transition from $\sqrt{19} \times \sqrt{19}$ to 2×2 happened as shown figure 2Sb. Once Te shutter was open, the 1×1 surface appeared as figure 2Sc. After scores of nms epitaxial growth of Bi_2Te_3 film, a set of RHEED pattern with Kikuchi lines appeared as figure 2Sd, indicating good crystal quality.

2. More AFM Investigations:

In order to further clarify the effect of the GaAs (111) surface on the growth mode of as-grown Q_2Te_3 films, more samples were grown, as shown in **Table 1S**. **Figure 3S** shows additional AFM results on the morphology of thicker Q_2Te_3 films grown on both V-GaAs (111)A and Nv-GaAs(111)A substrates. Figures 3S(a-c) are the AFM images of sample G, and it is very clear that the QL steps with a height of around 1 nm were formed over the whole surface, indicating that spiral growth mode can be maintained during the epitaxial growth of Q_2Te_3 film. Figure 3S(d-f) are the AFM images of sample H, and big terraces and steps were formed on the surface due to the step-flow growth mode. Even for samples I and J, with smaller miscut angle (2° and 1°), the step-bunched surface morphology was still kept, as shown in figures 3S(g-l).

Table 1S. Samples category of Q_2Te_3 on GaAs (111)A substrate

| Sample | Q_2Te_3 & Thickness | Buffer Layer & Thickness | Substrate[a] | Misalignment Angle | Conduction Type |
|--------|-------------------------------------|--------------------------|---|-------------------------|-----------------|
| G | Bi_2Te_3 & 100 nm | GaAs (111)A & 3 nm | Semi-insulating Nv-GaAs (111)A | $\pm 0.1^\circ$ | n |
| H | Bi_2Te_3 & 100 nm | GaAs (111)A & 3 nm | Semi-insulating V-GaAs (111)A $\rightarrow (\bar{2}11)$ | $3^\circ \pm 0.1^\circ$ | |
| I | Bi_2Te_3 & 100 nm | GaAs (111)A & 3 nm | Semi-insulating V-GaAs (111)A $\rightarrow (\bar{1}12)$ | $2^\circ \pm 0.1^\circ$ | |
| J | Bi_2Te_3 & 100 nm | GaAs (111)A & 3 nm | Semi-insulating V-GaAs (111)A $\rightarrow (\bar{1}\bar{1}2)$ | $1^\circ \pm 0.1^\circ$ | |

[a] Here, both V-GaAs (111)A and Nv-GaAs (111)A substrates were made by Wafer Technology Ltd.

3. Hall Bar

All the transport measurements are based on the same Hall bar structure as shown in figure 4S. Figure 4Sa is the schematic diagram (not proportional), and figure 4Sb is the corresponding optical microscopy image. The standard photo-lithography method was used for fabricating the Hall bar.^[2] Positive photoresist S1813 was spun at 4000 rpm for 45 seconds on Q_2Te_3 films, followed by 110 °C baking for 60 seconds. With a mask of Hall bar pattern, the photoresist-coated sample was exposed to ultraviolet light (365 nm wavelength) with exposure power of 8 mW/cm² for 7 seconds. The exposed part of the photoresist was removed after 40 seconds of developing (MF CD-26 developer). Then, bare area of Bi_2Te_3 film with no photoresist was wet-etched with 1 g of potassium dichromate in 10 ml of sulfuric acid and 520 ml of deionized (DI) water, whereas, diluted nitric acid (HNO_3 : H_2O = 1:1) was used for Sb_2Te_3 film. The expected etching rate for both Bi_2Te_3 and Sb_2Te_3 films is about 10 nm per minute, and DI water rinsing is needed.

4. Transport Properties of Q_2Te_3 films on GaAs (111)A Substrates

Figure 5S shows the typical transport data for Q_2Te_3 films on GaAs (111)A substrates. Low temperature Hall measurements indicates that samples B and D show p and n type conductivity, respectively, which support the conclusion that all the as-grown Sb_2Te_3 films show p type conducting behavior and all the as-grown Bi_2Te_3 films show n type conducting behavior. Similar to the case of Q_2Te_3 films on GaAs (111)B, nonlinear Hall behavior was also observed over 20 kOe for both samples B and D at 1.8 K, as shown in figures 5S(a-b), which is likely an indication of more than one transport channel (surface and bulk). Based on the linear behavior below 20 kOe, the carrier density can be estimated as $3.81 \times 10^{19} \text{cm}^{-3}$ and $2.04 \times 10^{19} \text{cm}^{-3}$ for samples B and D, respectively. Compared to the result in figure 4h, a stronger upturn was observed for sample B with fields 20 and 80 kOe, as shown in figure 5Sc. This is also observed for sample D below 10 K as show in figure 5Sd. In fact, figure 5Sd shows a typical temperature dependent MR measurement results for TIs in perpendicular magnetic field. The resistivity decreases from 210 K to 10 K, indicating a typical metallic behavior, whereas, the resistivity turns up with decreasing temperature below 10 K, which is reminiscent of the electron-electron interaction in TI films.^[3] Additionally, the WAL induced MR dip at small field was also observed for both sample B and D, as shown in figures 5S(e-f).^[3-7] It should be noted that the MR dip decreases with increasing temperature and disappears around 10 K, as shown in figure 5Sf, suggesting its quantum origin^[3]. The MR for three orientations of magnetic field was also measured at 1.8 K for both sample B and D, and it is obvious that the MR for perpendicular field is much higher than those for parallel fields, as shown in figures 5Sg-h. A near parabolic MR was observed for sample B in perpendicular magnetic field, and it is suppressed when the field is parallel to the current. However, a linear MR was observed for sample D with perpendicular field above 30 kOe, which may be attributed to the QLMR of the surface states^[8].

Reference

- [1] D. A. Woolf, D. I. Westwood, R. H. Williams 1993 *Semicond. Sci. Technol.* 8 1075
- [2] J. Wang, H. D. Li, C. Z. Chang, K. He, J. S. Lee, X. C. Ma, N. Samarth, Q. K. Xue, M. H. Xie, M. H. W. Chan, arXiv:1108.1465v1, [cond-mat.mtrl-sci].
- [3] J. Wang, A. M. DaSilva, C. Z. Chang, K. He, J. K. Jain, N. Samarth, X. C. Ma, Q. K. Xue, M. H. W. Chan 2011 *Phys. Rev. B* 83 245438
- [4] H. Z. Lu, J. R. Shi, S. Q. Shen 2011 *Phys. Rev. Lett.* 107 076801
- [5] Y. S. Kim, M. Brahlek, N. Bansal, E. Edrey, G. A. Kapilevich, K. Iida, M. Tanimura, Y. Horibe, S. W. Cheong, S. Oh 2011 *Phys. Rev. B* 84 073109

- [6] J. Wang, C. Z. Chang, H. D. Li, K. He, D. M. Zhang, M. Singh, X. C. Ma, N. Samarth, M. H. Xie, Q. K. Xue, M. H. W. Chan 2012 *Phys. Rev. B* 85 045415
- [7] H. T. He, G. Wang, T. Zhang, I. K. Sou, G. K. L. Wong, J. N. Wang, H. Z. Lu, S. Q. Shen, F. C. Zhang 2011 *Phys. Rev. Lett.* 106 166805
- [8] H. Tang, D. Liang, R. L. J. Qiu, X. P. A. Gao 2011 *Acs Nano* 5 7510

Figure Caption:

Figure 1S. RHEED patterns taken from a,b) GaAs (111)A-(2×2) after deoxidizing and the growth of buffer layer, c,d) GaAs (111)A after Te predeposition, and e,f) Bi₂Te₃ epilayer after scores of nms growth.

Figure 2S. RHEED patterns taken from a) GaAs (111)B-($\sqrt{19} \times \sqrt{19}$) right after the growth of buffer layer at 590 °C, b) GaAs (111)B (2×2) after cooling down to 250 °C, c) GaAs (111)B (1×1) after Te predeposition, and d) Bi₂Te₃ epilayer after scores of nms epitaxial growth.

Figure 3S. AFM images of surface morphology for as-grown Q₂Te₃ films. a) Sample G in 5×5 μm², b) Sample G in 500 nm×500 nm, c) the line profile corresponding to the line in b), d) Sample H in 5×5 μm², e) Sample H in 2×2 μm², f) the line profile corresponding to the line in e), g) Sample I in 5×5 μm², h) Sample I in 2×2 μm², i) the line profile corresponding to the line of h), j) Sample J in 5×5 μm², k) Sample J in 2×2 μm², l) the line profile corresponding to the line in k).

Figure 4S. Hall bar schematic diagram (not proportional) a) and the corresponding optical microscopy image b).

Figure 5S. Transport properties of as-grown Q₂Te₃ films on GaAs (111)A substrates. a,b) Hall resistance versus magnetic field (black solid line) at 1.8 K for samples B and D, respectively, and the red solid line is the linear fit, c) MR change versus temperature in different perpendicular magnetic field for sample B, d) MR change versus temperature (from 210 K to 1.8 K) in perpendicular magnetic field for sample D, e) Magnetoresistivity change for sample B in perpendicular magnetic fields configuration at 1.8 K, f) MR change for sample D in perpendicular magnetic fields configuration at three different temperature, g,h) MR change in both perpendicular and parallel magnetic fields configuration for samples B and D at 1.8 K, and the violet line is the linear fit. We use three different magnetic field configurations, H_⊥ denote magnetic field perpendicular to the surface of the thin film, while H_∥ and H_∥' denote an in-plane magnetic field perpendicular to and parallel to the excitation current, respectively.

Figures:

Figure 1S

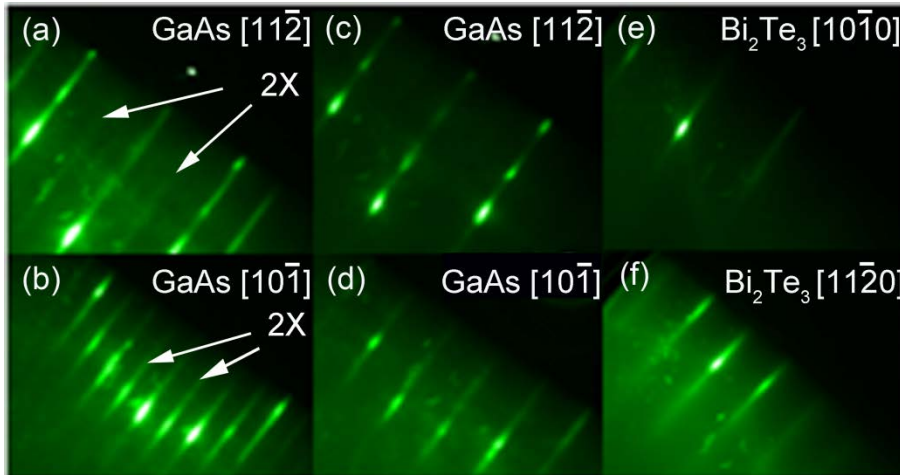


Figure 2S

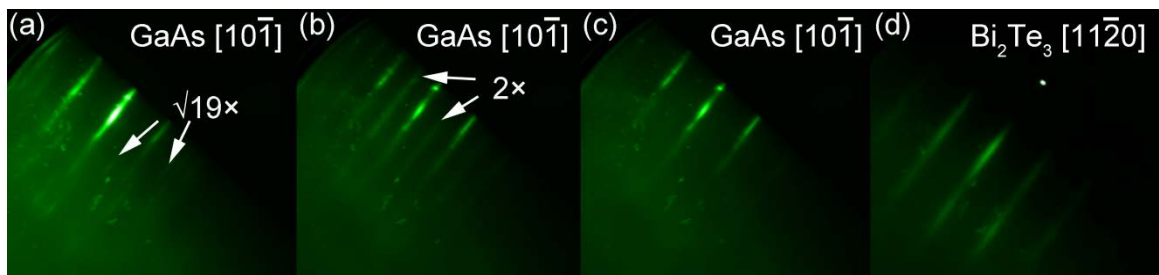


Figure 3S

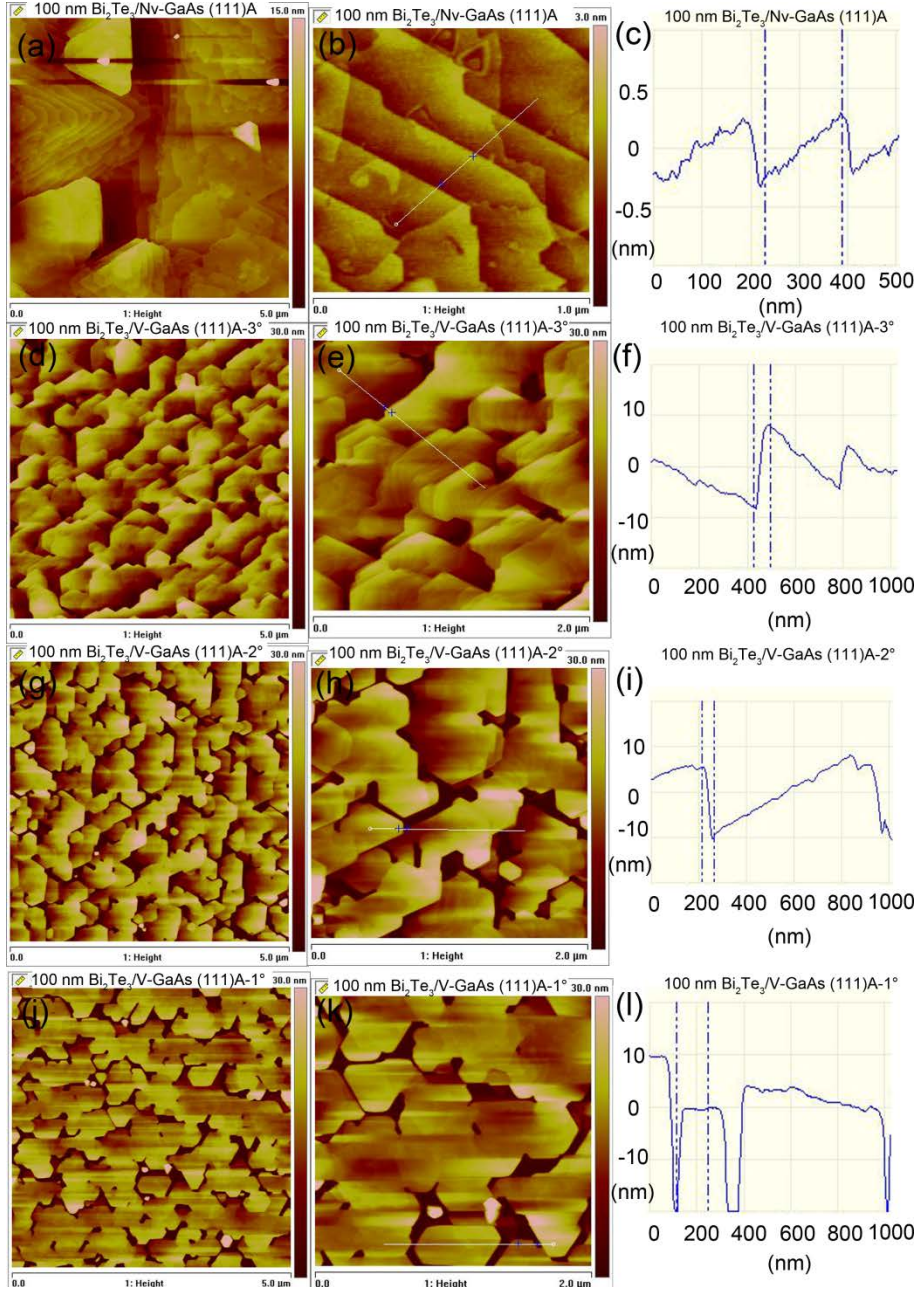


Figure 4S

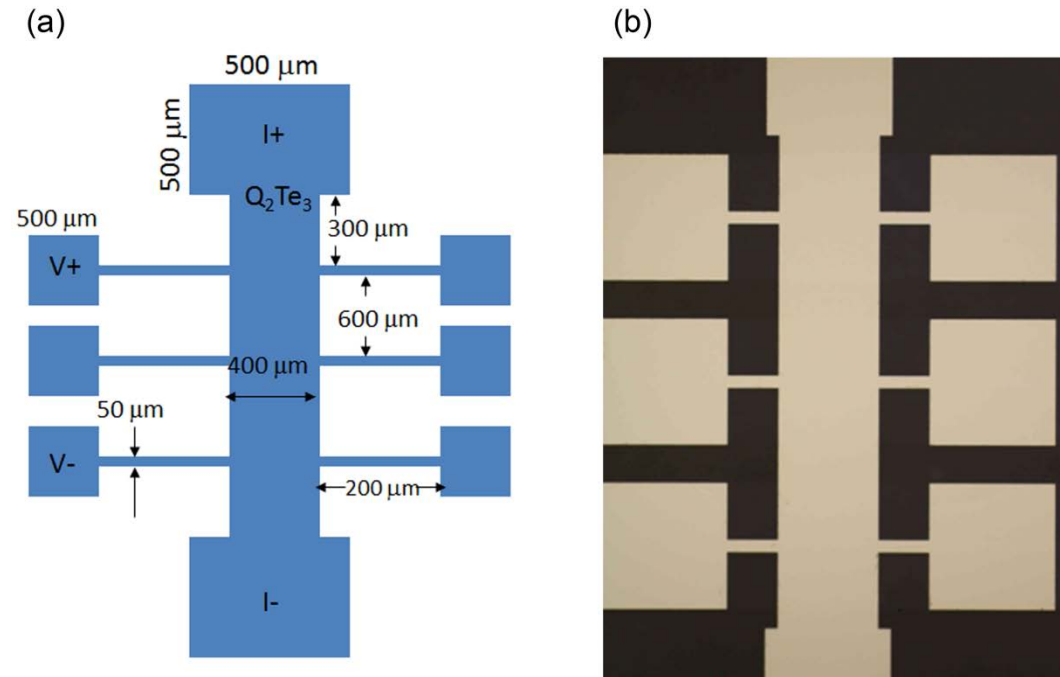


Figure 5S

